Probing the Excited States of Ru(II) Complexes with Dipyrido[2,3-a:3′,2′-c]phenazine: A Transient Resonance Raman Spectroscopy and Computational Study

Sarah L. Howell,[†] Keith C. Gordon,*[,†] and John J. McGarvey[‡]

MacDiarmid Institute for Advanced Materials and Nanotechnology, Department of Chemistry, University of Otago, Union Place, Dunedin, New Zealand, and School of Chemistry, Queen's University Belfast, Belfast BT9 5AG, Northern Ireland

Received: September 29, 2004; In Final Form: November 19, 2004

The lifetimes and transient resonance Raman spectra for Ru(II) complexes with the dipyrido[2,3-a:3′,2′-c]-phenazine (ppb) ligand and substituted analogues have been measured. The effect of altering the Ru(II) center ($\{Ru(CN)_4\}^{2-}$ versus $\{Ru(bpy)_2\}^{2+}$), of the complex, on the excited-state lifetimes and spectra has been considered. For $[Ru(bpy)_2L]^{2+}$ complexes the excited-state lifetimes range from 124 to 600 ns in MeCN depending on the substituents on the ppb ligand. For the $[Ru(CN)_4L]^{2-}$ complexes the lifetimes in H_2O are approximately 5 ns. The transient resonance Raman spectra for the MLCT excited states of these complexes have been measured. The data are analyzed by comparison with the resonance Raman spectra of the electrochemically reduced $[(PPh_3)_2Cu(\mu\text{-}L^{\bullet-})Cu(PPh_3)_2]^+$ complexes. The vibrational spectra of the complexes have been modeled using DFT methods. For experimental ground-state vibrational spectra of the complexes the data may be compared to calculated spectra of the ligand or metal complex. It is found that the mean absolute deviation between experimental and calculated frequencies is less for the calculation on the respective metal complexes than for the ligand. For the transient resonance Raman spectra of the complexes the observed vibrational bands may be compared with those of the calculated ligand radical anion, the reduced complex $[Ru(CN)_4L^{\bullet-}]^{3-}$, or the triplet state of the complex. In terms of a correlation with the observed transient RR spectra, calculations on the metal complex models offered no significant improvement compared to those based on the ligand radical anion alone. In all cases small structural changes are predicted on going from the ground to excited state.

I. Introduction

Ru(II) polypyridyl complexes have long held a fascination for researchers as they have the potential for incorporation into energy harvesting and other optoelectronic devices.[1−4] Critical to the success of using compounds in these applications is a clear picture of the nature of the excited state formed upon photoexcitation. For most metal polypyridyl complexes that are used in energy harvesting applications[5−8] the active excited state is a metal-to-ligand charge-transfer (MLCT) state in which the metal is formally oxidized and the ligand formally reduced.[9] Many studies have used resonance Raman spectroscopy to probe the transient species formed following photoexcitation.[1,10,11] This may be achieved by single-color pump−probe methodology,[12,13] in which the leading edge of a laser pulse populates the transient state and the trailing edge probes the scattering from the transient. The single-color protocol has been successfully used to examine transient species on the nanosecond[14,15] and picosecond time scales.[16] An alternate method is the two-color experiment in which the pump pulse creates the transient species and resonance Raman scattering is produced by the probe pulse—the delay between the arrival of each of these pulses at the sample may be used to give temporal resolution.[17] In the case of MLCT excited states the key spectral signatures that manifest in the resonance Raman spectra are often features of the ligand radical anion species.[12,16,18−20] For example Woodruff et al.,[12] in their seminal work on the resonance Raman excited-state spectrum of $[Ru(bpy)_3]^{2+}$, were able to show the presence of $bpy^{\bullet-}$ in the MLCT state by comparing the complexes excited-state spectrum with that of chemically generated $bpy^{\bullet-}$. The close correspondence between features in these two spectra provided strong evidence for $[Ru^{(III)}(bpy)_2(bpy^{\bullet-})]^{2+*}$ formulation of the MLCT excited state. In some cases the vibrational signatures from spectator ligands may also be observed, as is the case for tetracarbonyl(α-diimine)tungsten complexes studied by Zink et al.[21]

Many attempts have been made to model the MLCT excited states of polypyridyl complexes. Often reduction of a ligand is used as a model for excitation of a complex,[22] due to the nature of the excited state involving the formal oxidation of metal center and reduction of a ligand to its radical anion. One of the first detailed theoretical studies by Damrauer at el.[22] used ligand radical anions and even parts of ligands to explore the level of electron delocalization in MLCT excited states for a series of 5,5′-diphenyl-2,2′-bipyridine ligands and their complexes. Through studies of the aryl pyridine sections of the ligand it was possible to establish that the level of electron delocalization between phenyl and pyridine as the phenyl groups was substituted. The calculations on the reduced aryl pyridines showed that in the MLCT excited state the ligands would attempt to adopt a planar geometry with reorganization energies of between 4 and 7 kcal/mol for 4-phenylpyridine, 4-(o-tolyl)pyridine and 4-(2,6-dimethylphenyl)pyridine. Model complexes have also been used to approximate the excited state. Previous studies have shown

* Corresponding author e-mail: kgordon@alkali.otago.ac.nz.
† University of Otago.
‡ Queen's University Belfast.

10.1021/jp040637v CCC: $30.25
Published on Web 03/08/2005

SCHEME 1: Structure of ppb (R = H), $ppbMe_2$ (R = CH'_3), and $ppbCl_2$ (R = Cl)

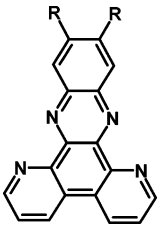

that the MLCT excited state of $[Cu(phen)(PPh_3)_2]^+$ can be modeled using B3LYP/6-31G(d) calculations on the reduced state of $[Cu(phen)(PH_3)_2]^+$.[23] Good agreement was found between the calculated modes and those observed in the transient resonance Raman spectrum. It was also found that the radical anion of phen alone, $phen^{\bullet-}$, was less effective at modeling the radical anion features present in the excited state of the complex $[Cu(phen)(PPh_3)_2]^+$.

The first example of the calculation of a molecular structure and vibrational spectra of an MLCT excited state of a polypyridyl complex was reported by Schoonover et al.[24] They investigated the MLCT excited state of $[Re(bpy)(CO)_3(4\text{-}Etpy)]^+$ (4Etpy = 4-ethylpyridine), using density functional theory, with the B3LYP method and a 6-31G(d) basis set on all atoms except Re. The Re atom was modeled using a modified LANL2DZ-type effective core potential (ECP) basis set.[24] The frequencies of the CO modes were calculated for the excited state and compared to those observed in time-resolved IR (TRIR) spectra. The shifts in the CO modes upon excitation are well reproduced by the calculation, as are the relative intensities of the bands in both the ground and excited states. The calculated geometry changes around the metal center upon excitation also support their predictions of molecular orbital mixing in the excited state.

We are interested in complexes with the dipyrido[2,3-a:3′,2′-c]phenazine (ppb) ligand and substituted analogues (Scheme 1). The ppb ligand is unusual in that it forms complexes with low-lying MLCT excited states which still possess long lifetimes.[25] For many polypyridyl complexes, low energy MLCT states have short lifetimes because of increased rates of nonradiative relaxation, k_{nr}, as expounded by Meyer et al.[8,26,27] In a study of the excited-state lifetimes of a series of complexes, including $[Ru(bpy)_2(ppb)]^{2+}$, Treadway et al.[25] were able to evaluate the structural distortion on going from ground to excited state, by analyzing the emission spectra of the complexes. This study provided evidence that the long-lived excited state for the ppb complex studied derived from the very small structural distortion attendant upon MLCT excitation; namely the ligand, having a delocalized electronic structure and being somewhat rigid, did not undergo large structural changes upon formation of the radical anion as part of the MLCT-state population. We have used transient resonance Raman spectroscopy to gain insight into the structural changes that occur with photoexcitation for a number of ppb-based complexes. We have also used spectral data from the spectroelectrochemistry of ppb complexes and density functional theory calculations on the vibrational spectra of $ppb^{\bullet-}$.[28] Calculations have also been carried out on the reduced states of $[Ru(CN)_4ppb]^{2-}$ and $[Ru(bpy)_2ppb]^{2+}$ as well as the excited state of $[Ru(CN)_4ppb]^{2-}$, in an attempt to improve the modeling of the corresponding excited states.

II. Methods

The syntheses of ppb, $ppbCl_2$ and $ppbMe_2$ have been previously described.[29]

$[Ru(bpy)_2L](PF_6)_2$ complexes were prepared based on methods previously published.[30] $[Ru(bpy)_2Cl_2]$ (104 mg, 0.2 mmol) and the polypyridyl ligand (0.31 mmol) were dissolved in 1:1 ethanol:water mixture (20 mL) and refluxed overnight. The solvent was removed from the solution by rotary evaporation. The resulting solid was dissolved in water (~10 mL) and filtered to remove unreacted ligand. Saturated $NaPF_{6(aq)}$ solution was added dropwise (~0.5 mL) until the complex precipitated out. The precipitate was filtered from the solution and recrystallized from methanol if required.

$K_2[Ru(CN)_4L]$ complexes were prepared using methods based on those previously published.[31] $K_4[Ru(CN)_6]\cdot xH_2O$ was used as supplied (Aldrich). $K_2[Ru(CN)_4L]$:$K_4[Ru(CN)_6]\cdot xH_2O$ (250 mg, 0.55 mmol, assuming 2 H_2O) in water (250 mL) was added to the polypyridyl ligand (0.50 mmol) in methanol (300 mL) in a quartz reaction vessel. The resulting solution was purged with argon and irradiated with 254 nm light for 30 h. The solvent was removed by rotary evaporation. The solid was dissolved in the minimum amount of water and filtered to remove unreacted polypyridyl ligand. Methanol (~150 mL) was added to the solution, and the solution was filtered to remove unreacted Ru(II) precursor. The solvent was removed from the filtrate by rotary evaporation. The solid was redissolved in a minimum amount of water and acetone was added (~150 mL). The solution was filtered, and the collected solid is $K_2[Ru(CN)_4L]$.

Microanalysis of $K_2[Ru(CN)_4L]$ complexes could not be carried out due to incomplete combustion.[32]

$[Ru(bpy)_2ppb](PF_6)_2$. Found: C, 43.84; H, 2.72; N, 10.64%. Calcd for $C_{38}H_{26}N_8P_2F_{12}Ru.(H_2O)_3$: C, 43.89; H, 3.10; N, 10.78%.

$[Ru(bpy)_2ppbCl_2](PF_6)_2$. Found: C, 40.02; H, 2.48; N, 9.54%. Calcd for $C_{38}H_{22}N_8Cl_2P_2F_{12}Ru.(H_2O)_{4.5}$: C, 40.19; H, 2.93; N, 9.87%.

$[Ru(bpy)_2(ppbMe_2)](PF_6)_2$. Yield: 84%; Found: C, 45.54; H, 2.96; N, 10.57%. Calcd for $C_{40}H_{30}N_8P_2F_{12}Ru.(H_2O)_2$: C, 45.76; H, 2.84; N, 10.61%.

$K_2[Ru(CN)_4(ppb)]$. Yield: 30%; ^{1}H NMR (500 MHz, D_2O) δ 9.48 (1H, d, J = 8.5 Hz), 9.16 (1H, d, J = 5.0 Hz), 8.11 (1H, d, J = 8.5 Hz), 7.93−7.74 (5H, m), 7.28 (1H, dd, J_1 = 5.5 Hz, J_2 = 2.5 Hz), 6.34 (1H, s); MS (ES) m/z 462 ({M−K_2−CN}$^-$).

$K_2[Ru(CN)_4(ppbCl_2)]$. Yield: 38%; ^{1}H NMR (500 MHz, D_2O) δ 9.81 (1H, s), 9.20 (1H, s), 8.22−7.86 (4H, m), 7.38 (1H, d, J = 4.5 Hz); MS (ES) m/z 557 ({MH−K_2}$^-$).

$K_2[Ru(CN)_4(ppbMe_2)]$. Yield: 26%; ^{1}H NMR (500 MHz, D_2O) δ 9.29 (1H, s), 9.16 (1H, d, J = 5.0 Hz), 8.16 (1H, d, J = 8.0 Hz), 7.95 (1H, d, J = 8.5 Hz), 7.86 (1H, s), 7.55 (1H, s), 7.28 (1H, dd, J_1 = 5.0 Hz, J_2 = 3.0 Hz), 6.47 (1H, s), 2.25 (3H, s), 2.16 (3H, s); MS (ES) m/z 517 ({MH−K_2}$^-$).

Spectroscopic grade solvents were used for all spectroscopic measurements.

Synthetic Analysis. ^{1}H NMR spectra were recorded at 25 °C, using a Varian 500 NMR spectrometer. Chemical shifts are given relative to residual solvent peaks. Microanalyses were performed at the Campbell Microanalysis Laboratory at the University of Otago. Mass spectrometry measurements were obtained from a Micromass LCT instrument. Electronic absorption spectra were recorded on a Varian Cary 500 scan UV−Vis−NIR spectrophotometer, with Cary WinUV software. Samples were typically ~10^{-4} mol dm^{-3}.

Experimental details for resonance Raman and transient resonance Raman measurements are detailed elsewhere.[23] Samples were 3 mol dm^{-3} in either distilled water ($[Ru(CN)_4L]^{2-}$ complexes) or acetonitrile ($[Ru(bpy)_2L]^{2+}$ complexes).

TABLE 1: Excited-State Lifetimes of Some Ru(II) Complexes of ppb, $ppbCl_2$, and $ppbMe_2$

complex	solvent	abs max/10^3 cm^{-1}	τ/ns[a]	τ/ns (lit.)
$[Ru(CN)_4(ppb)]^{2-}$	H_2O	19.1	<5	
$[Ru(CN)_4(ppbMe_2)]^{2-}$	H_2O	19.1	<5	
$[Ru(bpy)_2(ppb)]^{2+}$	CH_3CN	18.7	322	327[b]
$[Ru(bpy)_2(ppbCl_2)]^{2+}$	CH_3CN	17.9	124	
$[Ru(bpy)_2(ppbMe_2)]^{2+}$	CH_3CN	19.0	600	

[a] Excited-state lifetimes of $[Ru(CN)_4L]^{2-}$ complexes were measured with 355 nm excitation and those of the $[Ru(bpy)_2L]^{2+}$ complexes with 532 nm excitation. [b] Reference 25.

Transient lifetimes measurements were made using a nanosecond pulsed excitation source (Spectra-Physics Quanta-Ray, Model DCR Nd^{3+}/YAG laser). Transient absorption decay signals at various detection wavelengths were measured with a photomultiplier tube RCA 1P28 in which several of the dynodes were wired to the anode as in the circuit described by Hunt and Thomas[33] to provide rapid response. Kinetic traces were recorded using a digital oscilloscope (Tektronix model TDS 3032). All measurements were of approximately 0.05−0.1 mM solutions at room temperature. Solutions were purged with argon for 10 min prior to measurement. UV/Vis spectra were collected before and after emission lifetime measurements in order to check that no sample degradation had occurred. Incident pulse energies were typically ∼ 10 mJ. The transient lifetime was determined by fitting a single-exponential function to each signal. Transient decay signals were collected at 2−3 wavelengths for each sample, and the reported lifetimes are the mean of these measurements.

FT-IR spectra were collected, using a Perkin-Elmer Spectrum BX FT-IR system with Spectrum v.2.00 software, of potassium bromide (KBr) disks. Spectra were measured using 64 scans.

FT-Raman spectra were collected on solutions (10^{-3}−10^{-1} M), using a Bruker IFS-55 FT-interferometer bench equipped with an FRA/106 Raman accessory and utilizing OPUS (version 4.0) software. An Nd:YAG laser with 1064 nm excitation wavelength was used. An InGaAs diode (D424) operating at room temperature was used to detect Raman photons. Spectra were measured for 100 scans for the $[Ru(bpy)_2L]^{2+}$ complexes in acetonitrile and for 16 h for $[Ru(CN)_4L]^{2-}$ complexes in water, at a output power of 450 mW, with a resolution of 4 cm^{-1}.

The geometries, vibrational frequencies, and their IR and Raman intensities were calculated using DFT calculations (B3LYP functional) with the basis set 6-31G(d) on the ligands and an effective core potential (ECP) with the LANL2DZ basis set on the Ru(II) atom. These were implemented with Gaussian 03W.[34] Atomic charges were determined using natural population analysis (NPA) calculations on the optimized structures using the above basis sets. The visualization of the vibrational modes and molecular orbitals was provided by GaussViewW 3.09 (Gaussian Inc.).

III. Results

Ru(II) complexes of ppb and the substituted analogues, $ppbCl_2$ and $ppbMe_2$, were investigated using transient resonance Raman spectroscopy with 355 nm excitation. Two different Ru(II) centers were considered, $\{Ru(bpy)_2\}^{2+}$ and $\{Ru(CN)_4\}^{2-}$, in order to determine the effect of the different metal moieties on the transient resonance Raman spectra, excited-state structures, and excited-state lifetimes.

III. a. Excited-State Lifetimes. The excited-state lifetimes were measured using excited-state absorption (Table 1). The lifetimes for the $[Ru(CN)_4L]^{2-}$ complexes in water were found to be significantly shorter than the $[Ru(bpy)_2L]^{2+}$ complexes in acetonitrile. The excited-state lifetimes of $[Ru(CN)_4ppb]^{2-}$ and $[Ru(CN)_4ppbMe_2]^{2-}$ in water were found to be comparable to the pulse duration of the experiment (∼5−7 ns) as the excited-state signal could not be deconvoluted from that of the laser scatter. The excited-state lifetime of $[Ru(CN)_4ppbCl_2]^{2-}$ could not be measured using the described experimental set up as the excited state is too short-lived to be detected. $[Ru(bpy)_2ppb]^{2+}$ was found to have an excited-state lifetime of 322 ns in acetonitrile, in agreement with the previous findings.[25] The excited-state lifetime of $[Ru(bpy)_2ppbCl_2]^{2+}$ was found to be 124 ns and that of $[Ru(bpy)_2ppbMe_2]^{2+}$ was found to be 600 ns. The variation in the excited-state lifetimes of the complexes upon substitution of ppb is consistent with the energy gap law.[25,35−37] The significant increase in the lifetimes of the $[Ru(bpy)_2L]^{2+}$ compared to the $[Ru(CN)_4L]^{2-}$ complexes can be attributed to the bulky bpy ligands shielding the metal center from solvent interaction in the excited state.

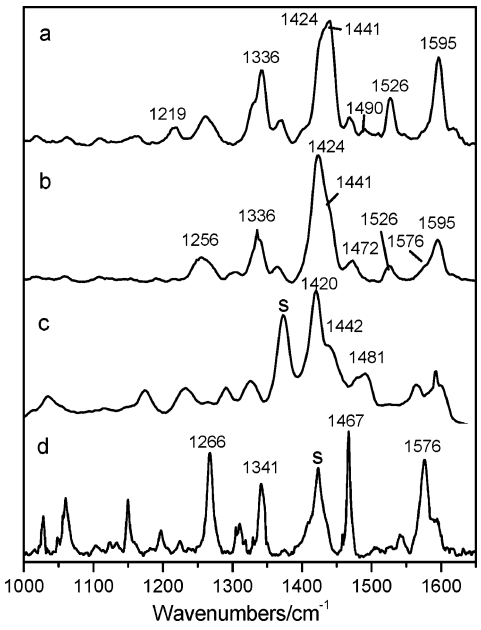

Figure 1. (a) RR spectrum of $[Ru(CN)_4ppb]^{2-}$ (356 nm CW excitation) in H_2O (3 mM). (b) Transient resonance Raman spectrum of $[Ru(CN)_4ppb]^{2-}$ (355 nm pulsed excitation, 3.6 mJ per pulse) in H_2O (3 mM). (c) Transient resonance Raman spectrum of $[Ru(bpy)_2ppb]^{2+}$ (355 nm pulsed excitation) in CH_3CN (3 mM). (d) RR spectrum of $[(PPh_3)_2Cu(\mu\text{-}ppb^{\bullet-})Cu(PPh_3)_2]^+$ (514 nm CW excitation) in CH_2Cl_2 (3 mM, 0.1 M TBAP electrolyte) (from ref 28). s denotes a solvent band.

III. b. Transient Resonance Raman Data. The transient resonance Raman spectra of $[Ru(bpy)_2ppb]^{2+}$, $[Ru(bpy)_2ppbCl_2]^{2+}$, and $[Ru(bpy)_2ppbMe_2]^{2+}$ were collected using 355 nm excitation at a series of pulse powers (Figure 1, Tables 2 and 3).[38] The spectra remain unchanged as a function of laser power, suggesting that a single state is being probed in these experiments. We attribute these spectra to the MLCT states of the respective complexes. The spectra generated using pulsed excitation differ from their respective ground-state spectra in the frequencies and intensities of the bands. For each of the complexes at least one ground-state band is bleached in the spectra generated with pulsed excitation, supporting the assignment of the spectra as being due to the excited state of the complexes.[39] $[Ru(bpy)_2ppb]^{2+}$ shows bleaching of bands at several bands: two in the 1000−1650 cm^{-1} range at 1210 and 1260 cm^{-1}, with others at lower frequencies. $[Ru(bpy)_2ppbCl_2]^{2+}$ exhibits bleaching of ground-state features at 754 and 1521 cm^{-1} and $[Ru(bpy)_2ppbMe_2]^{2+}$ at 1346 cm^{-1}.

TABLE 2: Calculated Vibrational Bands of ppb$^{\bullet-}$, [Ru(CN)$_4$(ppb$^{\bullet-}$)]$^{3-}$, and [Ru(CN)$_4$ppb]$^{2-}$*, Wavenumbers of Bands from the Transient Resonance Raman Spectra of [Ru(CN)$_4$ppb]$^{2-}$ and [Ru(bpy)$_2$ppb]$^{2+}$ (355 nm Pulsed Excitation), and the Resonance Raman Spectrum of [(PPh$_3$)$_2$Cu(μ-ppb$^{\bullet-}$)Cu(PPh$_3$)$_2$]$^+$ (514 nm CW Excitation)

ppb$^{\bullet-}$ calculated[a]		[Ru(CN)$_4$(ppb$^{\bullet-}$)]$^{3-}$ calculated[b]		[Ru(CN)$_4$ppb]$^{2-}$* calculated[b]	[Ru(CN)$_4$ppb]$^{2-}$* expt	[Ru(bpy)$_2$ppb]$^{2+}$* expt	[(Cu(PPh$_3$)$_2$)$_2$ppb$^{\bullet-}$]$^+$ expt[a]
mode number[c]	symmetry	$\tilde{\nu}$/cm^{-1}	$\tilde{\nu}$/cm^{-1}	$\tilde{\nu}$/cm^{-1}	ν/cm^{-1}	$\tilde{\nu}$/cm^{-1}	$\tilde{\nu}$/cm^{-1}
48	a$_1$	1022	1027	1032		1035	1027
49	a$_1$	1041	1035	1047			1059
50	b$_2$	1055	1063	1069			
51	a$_1$	1075	1078	1088			
52	b$_2$	1105	1107	1114			
53	a$_1$	1121	1113	1128			
54	b$_2$	1123	1115	1127			
55	a$_1$	1144	1137	1150			1149
56	b$_2$	1170	1157	1187			
57	a$_1$	1192	1190	1197			1197
58	b$_2$	1192	1214	1222			
59	a$_1$	1242	1252	1243		1232	
60	b$_2$	1249	1246	1254			
61	a$_1$	1277	1276	1275	1256		1266
62	b$_2$	1288	1284	1296			
63	b$_2$	1305	1305	1299			
64	a$_1$	1311	1310	1330	1303	1290	1310
65	a$_1$	1330	1337	1322	1336		1341
66	a$_1$	1347	1331	1348			
67	b$_2$	1348	1349	1342			
68	a$_1$	1376	1376	1390	1364		
69	a$_1$	1395	1390	1406	1424	1420	
70	b$_2$	1421	1415	1426			
71	a$_1$	1452	1437	1462	1441	1442	1467
72	b$_2$	1456	1451	1459			
73	b$_2$	1466	1460	1472			
74	a$_1$	1501	1484	1506	1472	1481	
75	a$_1$	1509	1493	1518	1526		
76	b$_2$	1546	1547	1556			
77	a$_1$	1557	1549	1563	1576		1576
78	b$_2$	1577	1582	1582			
79	b$_2$	1586	1573	1589			
80	a$_1$	1588	1560	1595	1595		1594

[a] Reference 28. [b] Calculated frequencies have been scaled by 0.973. [c] Mode number and symmetry label based from the ppb$^{\bullet-}$ calculation

TABLE 3: Wavenumbers of Bands from Transient Resonance Raman Spectra of [Ru(bpy)$_2$ppbCl$_2$]$^{2+}$, [Ru(CN)$_4$ppbMe$_2$]$^{2-}$, and [Ru(bpy)$_2$ppbMe$_2$]$^{2+}$ (355 nm Pulsed Excitation) and Resonance Raman Spectra [(PPh$_3$)$_2$Cu(μ-ppbCl$_2^{\bullet-}$)Cu(PPh$_3$)$_2$]$^+$ (457 nm CW Excitation) and [(PPh$_3$)$_2$Cu(μ-ppbMe$_2^{\bullet-}$)Cu(PPh$_3$)$_2$]$^+$ (514 nm CW Excitation)

[Ru(bpy)$_2$ppbCl$_2$]$^{2+}$*	[(Cu(PPh$_3$)$_2$)$_2$(ppbCl$_2^{\bullet-}$)]$^{+a}$	[Ru(CN)$_4$ppbMe$_2$]$^{2-}$*	[Ru(bpy)$_2$ppbMe$_2$]$^{2+}$*	[(Cu(PPh$_3$)$_2$)$_2$(ppbMe$_2^{\bullet-}$)]$^{+a}$
1038			1036	
		1199		
1216	1214	1232	1218	
1254	1257	1264	1268	
1292	1298	1280	1286	
	1335	1335		1328
		1354		1347
		1384		
1421		1423	1418	1405
1442		1451	1447	
1472		1479	1476	1475
1519	1525	1520	1525	1523
	1569	1576		1576
	1588	1597		1597

[a] Reference 28.

The lowest MLCT excited states of these systems has the formula [Ru^{III}(bpy)$_2$L$^{\bullet-}$]*, where L is ppb, ppbCl$_2$, or ppbMe$_2$. The ppb-type ligands are much easier to reduce than bpy, and thus ppb acts as the electron acceptor in the lowest energy excited MLCT state.[28]

The excited-state spectra for the three [Ru(bpy)$_2$L]$^{2+}$ complexes have many similarities. This is partially due to the significant spectral contribution from bpy modes, possibly enhanced through a ligand-to-metal charge-transfer transition (Ru(III)←bpy).[12] Bands due to bpy modes are observed around 1173, 1326, 1490, 1565, and 1595 cm^{-1} in the three spectra. The remainder of the bands observed in the spectra may be attributed to the radical anion of ppb and its substituted analogues (Tables 2 and 3). The three complexes have a series of bands in common due to ppb$^{\bullet-}$ and substituted analogues, observed at 1035, 1290, 1420, 1442, and 1481 cm^{-1} for [Ru(bpy)$_2$ppb]$^{2+}$, shifting by up to 9 cm^{-1} in the substituted analogues. The transient resonance Raman spectra of [Ru(bpy)$_2$ppbCl$_2$]$^{2+}$ and [Ru(bpy)$_2$ppbMe$_2$]$^{2+}$ show additional bands around 1216, 1254, 1325, and 1519 cm^{-1} for both complexes. The abundance of bpy modes in this region of the spectra may be obscuring additional ppb radical anion modes.

The $[Ru(bpy)_2L]^{2+}$ complexes are challenging to study spectroscopically because of the strong signals from the ancillary bpy ligands. The $[Ru(CN)_4ppb]^{2-}$ complex is much simpler in this respect. The ancillary ligands in this complex are spectroscopically silent in the region of interest (1000−1650 cm^{-1}), which allows for a more straightforward identification of modes characteristic of $ppb^{\bullet-}$. An advantage of examining these two systems is that the effect of differing metal complex moieties may be probed.

The transient resonance Raman spectra of $[Ru(CN)_4ppb]^{2-}$ and $[Ru(CN)_4ppbMe_2]^{2-}$ were measured at 355 nm with pulse powers of ~3 mJ per pulse (Figure 1, Tables 2 and 3). Despite the comparatively short lifetimes for the excited states of these complexes, evidence of the formation of an excited-state comes from the differing intensity pattern, the shifting of bands compared to the respective ground-state spectra and also the bleaching of ground-state features.[40] The spectra of the ground and corresponding excited states show several bands at near identical frequencies; however, in the 1000−1650 cm^{-1} region, ground-state bands at 1219 and 1490 cm^{-1} are bleached in the transient resonance Raman spectrum of $[Ru(CN)_4ppb]^{2-}$, indicating complete conversion to the excited state. Ground-state bands at 1135 and 1375 cm^{-1} are bleached in the spectrum of $[Ru(CN)_4ppbMe_2]^{2-}$*. The transient resonance Raman spectra of these complexes show more bands due to $ppb^{\bullet-}$ and $ppbMe_2^{\bullet-}$, compared to the spectra of the $[Ru(bpy)_2L]^{2+}$ complexes. The two $[Ru(CN)_4L]^{2-}$ complexes have a series of similar bands at 1335, 1424, 1441, 1472, 1526, 1576, and 1595 cm^{-1} for the ppb complex, typically increasing in frequency by up to 10 cm^{-1}, for the $ppbMe_2$ complex. $[Ru(CN)_4ppb]^{2-}$ has a unique band at 1256 cm^{-1}, and $[Ru(CN)_4ppbMe_2]^{2-}$ has several unique bands at 1199, 1232, 1264, 1280, and 1384 cm^{-1}.

IV. Discussion

IV. a. Transient Resonance Raman Data. Comparison between the transient resonance Raman spectra of the $[Ru(bpy)_2L]^{2+}$ complexes with those of the $[Ru(CN)_4L]^{2-}$ complexes shows that the excited-state complexes have some modes in common (Figure 1, Tables 2 and 3). The transient resonance Raman spectra of $[Ru(bpy)_2ppb]^{2+}$ and $[Ru(CN)_4ppb]^{2-}$ have four bands in common, observed at 1290, 1420, 1442, and 1481 cm^{-1} for the $[Ru(bpy)_2ppb]^{2+}$ complex. These lie at 1303, 1421, 1446, and 1490 cm^{-1}, respectively, in the $[Ru(CN)_4ppb]^{2-}$ spectrum. The $ppbMe_2$ complexes show a greater number of bands in common in the transient resonance Raman spectra. These are observed at 1218, 1268, 1286 1418, 1447, 1476, and 1525 cm^{-1} in the spectrum of $[Ru(bpy)_2ppbMe_2]^{2+}$*. For most of the bands the frequencies increase in the $[Ru(CN)_4ppbMe_2]^{2-}$* spectrum, by up to 6 cm^{-1}. The band at 1218 cm^{-1} in the spectrum of $[Ru(bpy)_2ppbMe_2]^{2+}$* exhibits a significant increase in frequency of 14 cm^{-1} in the spectrum of $[Ru(CN)_4ppbMe_2]^{2-}$*.

The bands observed in the transient resonance Raman spectra of these Ru complexes can also be compared to the previously published resonance Raman spectra of the reduced binuclear Cu(I) complexes of ppb, $ppbCl_2$, and $ppbMe_2$, $[(PPh_3)_2Cu(\mu\text{-}ppb^{\bullet-})Cu(PPh_3)_2]^+$, $[(PPh_3)_2Cu(\mu\text{-}ppbCl_2^{\bullet-})Cu(PPh_3)_2]^+$, and $[(PPh_3)_2Cu(\mu\text{-}ppbMe_2^{\bullet-})Cu(PPh_3)_2]^+$, and to calculations carried out on $ppb^{\cdot-}$ and its substituted analogues (B3LYP/6-31G(d)) (Figure 1, Tables 2 and 3, and Supporting Information Table S1).[28] The resonance Raman spectrum of $[(PPh_3)_2Cu(\mu\text{-}ppb^{\bullet-})Cu(PPh_3)_2]^+$, which has bands characteristic of $ppb^{\bullet-}$, appears to have more similarities to the transient resonance Raman spectrum of $[Ru(CN)_4ppb]^{2-}$ than that of $[Ru(bpy)_2ppb]^{2+}$. This may be due to the absence of the bands owing to the bpy ligands. They have a series of bands in common, observed at 1266, 1310, 1341, 1467, 1576, and 1594 cm^{-1} for $[(PPh_3)_2Cu(\mu\text{-}ppb^{\bullet-})Cu(PPh_3)_2]^+$. The intensity patterns for the two spectra are quite different, but this can be attributed to the different metal centers and the difference in resonance enhancement, due to the choice of excitation wavelength in each experiment. In the spectrum of $[Ru(CN)_4ppb]^{2-}$*, these bands are typically observed within 10 cm^{-1} of those for the Cu complex. These modes can then in turn be correlated to the calculated modes of $ppb^{\bullet-}$. The most significant difference, between the resonance Raman spectrum of $[(PPh_3)_2Cu(\mu\text{-}ppb^{\bullet-})Cu(PPh_3)_2]^+$ and that of $[Ru(CN)_4ppb]^{2-}$*, is the band corresponding to ν_{71}. This lies at at 1467 cm^{-1} in the spectrum of $[(PPh_3)_2Cu(\mu\text{-}ppb^{\bullet-})Cu(PPh_3)_2]^+$ and is shifted to 1441 cm^{-1} in the spectrum of $[Ru(CN)_4ppb]^{2-}$*. There are a series of bands unique to the Cu complex and also a series of bands unique to the Ru complexes. These bands for the Ru complexes can also be matched to the calculated $ppb^{\bullet-}$ modes. The mean absolute deviation between the observed bands in the transient resonance Raman spectrum and those calculated for $ppb^{\bullet-}$ is 16 cm^{-1}. This may be due to effects of the metal center; first the presence of the metal center changes band frequencies, and in the MLCT excitation the charge transfer will not result in the reduction of ppb by 1.0 electron but a smaller part thereof.[13]

For the $ppbMe_2$ complexes, again the reduced Cu complex is most readily compared to the $[Ru(CN)_4L]^{2-}$ complex (Table 3). All the modes observed for $[(PPh_3)_2Cu(\mu\text{-}ppbMe_2^{\bullet-})Cu(PPh_3)_2]^+$ are seen in the transient resonance Raman spectrum of $[Ru(CN)_4ppbMe_2]^{2-}$. The correlated bands lie at similar frequencies or are shifted up in frequency (by up to 18 cm^{-1}) on going from the reduced Cu complex to the excited-state Ru complex. The transient resonance Raman spectrum of $[Ru(bpy)_2ppbMe_2]^{2+}$ has a number of additional features not observed in the spectrum from $[(PPh_3)_2Cu(\mu\text{-}ppbMe_2^{\bullet-})Cu(PPh_3)_2]^+$; however, these may be correlated to the calculated modes of $ppbMe_2^{\bullet-}$ (Supporting Information Table S1).

In the case of the spectrum of $[(PPh_3)_2Cu(\mu\text{-}ppbCl_2^{\bullet-})Cu(PPh_3)_2]^+$, comparison can be made to the $[Ru(bpy)_2ppbCl_2]^{2+}$ transient resonance Raman spectrum (Table 3) since the excited-state lifetime of the $[Ru(CN)_4ppbCl_2]^{2-}$ was too short to establish appreciable excited-state population with our single-color pump−probe protocol. These spectra have four bands in common, observed at 1216, 1254, 1292, and 1519 cm^{-1}, in the transient resonance Raman spectrum and are within 6 cm^{-1} of the bands for the Cu complex. As for the other Ru complexes, the bands in the spectrum of $[Ru(bpy)_2ppbCl_2]^{2+}$* can be correlated to the calculated $ppbCl_2^{\bullet-}$ modes (Supporting Information Table S2).

IV. b. Calculated Structures and Spectra. The initial modeling of the excited-state spectral properties of the complexes used the radical anion of the ligand to provide spectral signature information. To improve the calculated frequencies for these excited-state spectra, metal centers were incorporated into the calculation. The optimized geometries and vibrational modes of the ground states and reduced states of $[Ru(CN)_4ppb]^{2-}$ and $[Ru(bpy)_2ppb]^{2+}$ were computed using the B3LYP functional with the 6-31G(d) and LANL2DZ ECP basis sets. These calculations were carried out in order to account for the contribution of the metal center to the frequencies of vibration. The reduced state of a complex has been shown previously to be a reasonable model, both experimentally and computationally, for an MLCT excited state.[23,41−43] The lowest triplet state of $[Ru(CN)_4ppb]^{2-}$ was also calculated in order to establish whether this improves the quality of the excited-state model.

TABLE 4: Selected Calculated Bond Lengths for ppb and Ru(II) Complexes and Their Reduced States and $[Ru(CN)_4ppb]^{2-*}$ [a]

$Ru(CN)_4ppb]^{2-}$ calcd		$[Ru(bpy)_2ppb]^{2+}$ calcd			$[Ru(CN)_4(ppb^{\bullet-})]^{3-}$ calcd		$[Ru(CN)_4ppb]^{2-*}$ calcd		$[Ru(bpy)_2(ppb^{\bullet-})]^{+}$ calcd	
nonchelating side	chelating side	nonchelating side	chelating side	$ppb^{\bullet-}$ calcd	nonchelating side	chelating side	nonchelating side	chelating side	nonchelating side	chelating side
1.35	1.36	1.34	1.36	1.36	1.37	1.37	1.36	1.37	1.35	1.38
1.33	1.34	1.33	1.34	1.32	1.31	1.34	1.32	1.33	1.32	1.34
1.40	1.39	1.41	1.40	1.41	1.41	1.40	1.41	1.40	1.41	1.39
1.39	1.39	1.38	1.39	1.38	1.39	1.39	1.38	1.38	1.38	1.40
1.41	1.40	1.41	1.41	1.41	1.40	1.41	1.41	1.40	1.41	1.40
1.42	1.42	1.42	1.42	1.43	1.44	1.42	1.43	1.43	1.42	1.43
1.46		1.46		1.45	1.45		1.45		1.46	
1.47	1.44	1.47	1.45	1.46	1.44	1.45	1.46	1.43	1.48	1.42
1.43		1.43		1.43	1.44		1.43		1.43	
1.33	1.36	1.32	1.35	1.35	1.35	1.35	1.34	1.36	1.32	1.38
1.36	1.38	1.34	1.37	1.37	1.36	1.39	1.37	1.38	1.37	1.38
1.44		1.44		1.44	1.44		1.44		1.44	
1.42	1.42	1.43	1.42	1.41	1.42	1.41	1.41	1.41	1.41	1.41
1.38	1.38	1.37	1.38	1.39	1.39	1.39	1.39	1.39	1.38	1.39
1.41		1.42		1.40	1.40		1.40		1.40	

[a] Bond labels are defined in Figure 2.

The optimized geometry of $[Ru(CN)_4ppb]^{2-}$ was compared to the optimized geometry of ppb (Table 4).[28] The formation of a mononuclear complex causes a loss of symmetry in the ligand. While the bonds on the nonchelating side of ppb in the complex are within 0.01 Å of the uncomplexed ligand, those on the coordinating side of the ligand are changed by up to 0.03 Å. The largest changes are seen in r_8, r_{10}, and r_{11}, bonds (on the coordinating side) all close to the coordinated metal center. Bonds r_8, r_{10}, and r_{11} are also computed to undergo change upon complexation in $[Ru(CN)_4ppbMe_2]^{2-}$ and $[Ru(CN)_4ppbCl_2]^{2-}$ (Supporting Information Table S3). The structure calculated for $ppbCl_2$ is in agreement with the crystal structure of $[(PPh_3)_2Cu(\mu\text{-}ppbCl_2)Cu(PPh_3)_2]^{2+}$;[28] that is there are no large perturbations to the structure of $ppbCl_2$ in the complex that can be attributed to coordination to Cu(I). $\{Cu(PPh_3)_2\}^{+}$ moieties are typically not structurally demanding on coordinated ligands.[44]

The predicted vibrational spectra for the $[Ru(CN)_4ppb]^{2-}$ complexes show a closer correspondence to the experimental data than the ppb calculations (Table 5). For $[Ru(CN)_4ppb]^{2-}$ the calculated spectral data show a mean absolute deviation from experimental data of 9 cm^{-1}, this compares to 13 cm^{-1} for comparison of calculated ppb with experimental $[Ru(CN)_4ppb]^{2-}$ data. The respective mean absolute deviations for $[Ru(CN)_4ppbMe_2]^{2-}$ are 7 and 13 cm^{-1} (Supporting Information Table S4) There is also an improvement in band intensity correlation with incorporation of the metal center. These improvements suggested that modeling the reduced and excited states with calculations on the Ru(II) complexes would provide greater insight into the excited state therefore justifying the additional computational cost.

Comparison of the calculated structure of $[Ru(CN)_4(ppb^{\bullet-})]^{3-}$, the reduced state of $[Ru(CN)_4ppb]^{2-}$, to that of $ppb^{\bullet-}$, shows that incorporation of the Ru(II) center elongates r_2 and r_{11} on the coordinating side by 0.02 Å (Table 4). For $[Ru(CN)_4(ppbMe_2^{\bullet-})]^{3-}$, the reduced state of $[Ru(CN)_4ppbMe_2]^{2-}$, similar changes are seen from $ppbMe_2^{\bullet-}$ (Supporting Information Table S3). In the triplet-state calculation of $[Ru(CN)_4ppb]^{2-}$ (Table 4) the significant bond change from $ppb^{\bullet-}$ is in r_8 on the coordinating side. In the excited state this bond is 1.43 Å, 0.03 Å shorter than for $ppb^{\bullet-}$.

Reduction of ppb to its radical anion causes a change in bond lengths of up to 0.02 Å (Table 4). Reduction of $[Ru(CN)_4ppb]^{2-}$ causes changes in bond length up to 0.03 Å, with the largest changes being in r_8 and r_{10} on the noncoordinating side. This is similar to the calculated changes upon reduction of $[Ru(CN)_4ppbMe_2]^{2-}$ (see Supporting Information Table S3), with bond length changes upon of up to 0.03 Å, with the largest change calculated for r_8.

Calculation of the triplet state of $[Ru(CN)_4ppb]^{2-}$ shows little difference to the structure of the reduced state of $[Ru(CN)_4ppb]^{2-}$ (Table 4). The only bond predicted to have a difference of more than 0.01 Å compared to the reduced state is r_8, suggesting that the effect of a Ru(III) compared to a Ru(II) center is not great, in accord with the NPA calculations (see below). Interestingly the changes in bond length compared to the ground-state molecule are no more than 0.01 Å, smaller than the changes predicted for the reduction. This is consistent with the idea that the MLCT excitation transfers a fraction of 1 electron from the dπ metal MO to the π^* ppb MO.[13]

Further insight into the effect of reduction and photoexcitation on the $[Ru(CN)_4ppb]^{2-}$ may be obtained from an NPA calculation. The NPA calculation on $[Ru(CN)_4ppb]^{2-}$ shows that most of the -2 charge of this species is partitioned on the $\{Ru(CN)_4\}^{2-}$ moiety (-1.86) with only -0.14 on the ppb ligand. However for the reduced complex, $[Ru(CN)_4(ppb^{\bullet-})]^{3-}$, the ppb ligand holds -0.87 of the charge. The calculation for the excited-state complex reveals that the charge reallocation gives less negative charge to the ligand (-0.60) with the metal moiety having a charge of -1.40. The charge reallocation between ground and triplet state indicates extensive mixing between the formal donor, metal dπ, MO and acceptor, ppb π^*, MO. This mixing mitigates the full, 1 electron, oxidation of the metal moiety and full reduction of the ppb anticipated in an MLCT state.[9]

The bands observed in the transient resonance Raman spectrum of $[Ru(CN)_4ppb]^{2-}$ were compared to the calculated modes of $[Ru(CN)_4(ppb^{\bullet-})]^{3-}$ (Table 2). It was found that the prediction of some of the modes was improved by incorporation of the $\{Ru(CN)_4\}^{2-}$ moiety. In this calculation ν_{74} is predicted at 1484 cm^{-1}, compared to 1501 cm^{-1} for $ppb^{\bullet-}$, and is observed at 1472 cm^{-1}. However, ν_{80} is calculated at 1560 cm^{-1} for the reduced state but observed at 1595 cm^{-1}. The $ppb^{\bullet-}$ calculation more accurately predicts this at 1588 cm^{-1}. The mean absolute deviation in calculated modes for $[Ru(CN)_4(ppb^{\bullet-})]^{3-}$ and observed bands in the transient resonance Raman spectrum of $[Ru(CN)_4ppb]^{2-}$ is 20 cm^{-1}, *offering no improvement to the correlation of calculated and observed bands*, while increasing computational complexity. A similar observation can be made

TABLE 5: Calculated and Experimental Vibrational Data for ppb and $[Ru(CN)_4ppb]^{2}$

ppb calcd[a]				$[Ru(CN)_4ppb]^{2-}$ calcd[b]		$[Ru(CN)_4ppb]^{2-}$ expt[c]	
mode number[d]	symmetry	$\tilde{\nu}$/cm^{-1}	$\tilde{\nu}$/cm^{-1}	IR Int[e]	Ram Int	$\tilde{\nu}$/cm^{-1}	Ram Int[f]
48	a_1	1007	1024	1	7	1017	10
49	a_1	1055	1055	10	27	1060	21
50	b_2	1072	1073	6	3	1079	
51	a_1	1086	1090	6	3	1108	9
52	a_1	1126	1121	1	6		
53	b_2	1132	1129	9	2	1122	6
54	b_2	1135	1133	0	4	1146	4
55	a_1	1159	1151	3	3	1154	5
56	b_2	1207	1193	9	7		
57	a_1	1213	1207	17	6	1211	
59	a_1	1244	1226	11	32	1216	25
58	b_2	1237	1250	8	10	1251	16
60	a_1	1268	1257	31	35	1261	25
61	b_2	1288	1286	10	6		
62	b_2	1306	1298	3	25	1305	11
63	a_1	1322	1320	7	18		
65	b_2	1353	1333	14	35	1328	72
64	a_1	1349	1344	25	27	1369	
66	a_1	1360	1354	7	81	1341	69
67	a_1	1398	1395	77	6	1398	
68	a_1	1409	1398	18	100	1425	100
69	b_2	1433	1428	11	14		
70	b_2	1464	1448	9	81	1439	92
72	b_2	1488	1459	10	9	1468	33
71	a_1	1478	1476	6	7		
			1486	3	27	1487	17
73	a_1	1502	1500	43	13	1501	14
74	a_1	1548	1541	1	31	1571	44
76	a_1	1567	1555	100	39	1544	13
78	a_1	1606	1576	3	7		
77	b_2	1581	1578	22	22	1596	57
79	b_2	1610	1600	7	3		
80	b_2	1632	1621	1	2	1617	3

[a] Reference 28. [b] Calculated frequencies have been scaled by 0.973 for Ru complexes. [c] Experimental IR intensities not available due to a high background and broad bands in the IR spectrum. [d] Mode number and symmetry from the $ppb^{\bullet-}$ calculation. [e] Raman and IR intensities are normalized such that the most intense band in the region is given an intensity of 100 for both the calculated and observed intensities. [f] FT-Raman spectrum.

for the comparison of calculated modes of $[Ru(CN)_4(ppbMe_2^{\bullet-})]^{3-}$ to the spectrum of $[Ru(CN)_4ppbMe_2]^{2-*}$ (Supporting Information Table S1). Overall, incorporation of the $\{Ru(CN)_4\}^{2-}$ center has not improved the correlation between experimental observables and calculated vibrational spectra.

Comparison of the calculated triplet state, $[Ru(CN)_4ppb]^{2-*}$, modes to the transient resonance Raman spectrum of $[Ru(CN)_4ppb]^{2-}$ shows a reasonable agreement of the frequencies (Table 2). As in the case of the calculation of the reduced complex, $[Ru(CN)_4(ppb^{\bullet-})]^{3-}$, some bands are better predicted by the $[Ru(CN)_4ppb]^{2-*}$ calculation compared to the $ppb^{\bullet-}$ calculation, some are worse. For example, ν_{80} of $ppb^{\cdot-}$ is observed in the spectrum of $[Ru(CN)_4ppb]^{2-*}$ at 1595 cm^{-1} and is calculated at 1588 cm^{-1}, whereas in the $[Ru(CN)_4ppb]^{2-*}$ calculation this is predicted at 1595 cm^{-1}. ν_{64} of $ppb^{\bullet-}$ is calculated at 1311 cm^{-1} and is observed in the spectrum of $[Ru(CN)_4ppb]^{2-*}$ at 1303 cm^{-1}. However, for the triplet-state calculation this is predicted at 1330 cm^{-1}. The mean absolute deviation in the predicted values is 18 cm^{-1}. Overall, the triplet-state calculation has offered no improvement over the interpretation of the spectrum of $[Ru(CN)_4ppb]^{2-*}$ compared to the $ppb^{\bullet-}$ or the reduced Ru(II) complex calculations.

These comparisons have shown that inclusion of a $\{Ru(CN)_4\}^{2-}$ center in a calculation of the vibrational properties of $ppb^{\bullet-}$, both as the reduced complex and as the triplet state, has offered no increase in predictive power for the spectrum of $[Ru(CN)_4ppb]^{2-*}$, compared to considering the radical anion of ppb as a model for the MLCT excited state. Comparison of the bands in the spectrum of $[Ru(CN)_4ppb]^{2-*}$ to the bands seen in the resonance Raman spectrum of $[(PPh_3)_2Cu(\mu\text{-}ppb^{\bullet-})Cu(PPh_3)_2]^{+}$, shows that there is a perturbation to the vibrational modes from the Ru(II) center and/or the excited state versus reduced state, owing to a difference in the proportion of electron transferred. The calculated bands of $ppb^{\bullet-}$ correspond better to the reduced $[(PPh_3)_2Cu(\mu\text{-}ppb)Cu(PPh_3)_2]^{2+}$ bands, than those in the transient spectrum of $[Ru(CN)_4ppb]^{2-}$, with the mean absolute deviation between calculated and observed frequencies for the Cu complex being 10 cm^{-1}. This is to be expected as the Cu(I) center does not greatly perturb the system, as seen for the structure of $ppbCl_2$ in $[(PPh_3)_2Cu(\mu\text{-}ppbCl_2)Cu(PPh_3)_2]^{2+}$.[28] It is somewhat surprising that the incorporation of the $\{Ru(CN)_4\}^{2-}$ center, while predicting a slight change in structure, offers no improvement to the calculated modes, although it does predict shifts in the modes. However, the reasonable agreement between the calculated modes of $ppb^{\bullet-}$ and the bands observed in the spectrum of $[Ru(CN)_4ppb]^{2-*}$ offers some aid in interpreting the transient resonance Raman spectrum. This agreement supports the approximation that the radical anion of a polypyridyl ligand can often be used to model the MLCT excited state of corresponding complexes. Alongside this, the radical anion of $ppb^{\cdot-}$ has been shown to approximate the reduced state of ppb complexes.[28] The advantage for this case is that the reduced and MLCT excited states of ppb can be modeled by the same molecule despite the nature of the metal center, greatly simplifying computations. This simplification does not apply to all polypyridyl complexes.[23]

Incorporation of $\{Ru(bpy)_2\}^{2+}$ into the calculation causes the largest bond length changes for ppb to occur in the same bonds as for the $[Ru(CN)_4L]^{2-}$ complexes: r_8, r_{10}, and r_{11} on the chelating side (Table 4). However, these changes are smaller at ~0.02 Å. For $[Ru(bpy)_2ppb]^{2+}$ this small change in the ppb structure allows for the assignment of the ppb vibrations to a_1 and b_2 symmetry labels (based on C_{2v} symmetry of the ppb ligand).

Comparison of the optimized structure of $[Ru(bpy)_2ppb]^{2+}$ to its reduced state, $[Ru(bpy)_2(ppb^{\bullet-})]^{+}$, shows that the largest change in bond length upon reduction occurs to r_8 on the chelating side (Table 4). This bond decreases by 0.03 Å to 1.42 Å. This is a much larger reduction in bond length than occurs for ppb to $ppb^{\bullet-}$, where this bond decreases by 0.01 Å. In addition the ppb in the reduced complex shows significant asymmetry, with r_8 on the nonchelating side being 1.48 Å.

The NPA calculation for $[Ru(bpy)_2ppb]^{2+}$ shows that the +2 charge is located on both the metal (+0.60) and each of the ligands (+0.46 to +0.48). The calculation for the reduced species shows a significant alteration of the charge on the ppb ligand (from +0.46 to −0.32) with more modest *changes in charge* for the metal (+0.61) and ancillary ligands (+0.36 each).

The frequency calculations on $[Ru(bpy)_2ppb]^{2+}$ show three distinct types of normal mode of vibration: (1) modes in which the eigenvectors are localized on one of both the bpy ligands (bpy modes); (2) modes which are localized on the ppb ligand (ppb modes); and (3) modes in which the eigenvectors involve motion of both bpy and ppb ligands (delocalized modes). Details of the calculated results are provided (Supporting Information Table S4). In general all of the modes are also highly symmetrical, allowing easy prediction of those modes which have the potential to exhibit resonance enhancement. However, calculated modes for $[Ru(bpy)_2ppb^{\bullet-}]^{+}$ exhibit many delocalized modes, leaving few modes localized on one ligand type only (Supporting Information Table S5). Furthermore the ppb modes of $[Ru(bpy)_2ppb^{\bullet-}]^{+}$ are much less symmetrical than for the unreduced ligand, owing to the loss of symmetry in the ligand upon reduction of the complex. The five bpy modes identified in the transient resonance Raman spectrum of $[Ru(bpy)_2ppb]^{2+}$ at 1173, 1316, 1490, 1565, and 1599 cm^{-1} can be correlated to bpy-based[12] or combined bpy/ppb modes calculated at 1162/1166 ($\nu_{135/136}$), 1290/1296 ($\nu_{149/150}$), 1496(ν_{173}), 1551/1554-($\nu_{175/176}$), and 1599/1601 ($\nu_{182/183}$) cm^{-1}, respectively (Figure 1, Table 2). The modes identified as being due to ppb are observed at 1035, 1232, 1290, 1420, 1442, and 1481 cm^{-1}. Most of these bands are in reasonable agreement with modes calculated for $[Ru(bpy)_2ppb^{\bullet-}]^{+}$ at 1029/1030 ($\nu_{115/116}$), 1248 (ν_{140}), 1316 (ν_{154}), 1390 (ν_{159}), 1447(ν_{165}), and 1521 (ν_{174}). These modes are delocalized but have most of the their eigenvector magnitude on the ppb ligand.

The frequencies of bands observed in the transient resonance Raman spectrum of $[Ru(bpy)_2ppb]^{2+}$ and those calculated for either the reduced complex, $[Ru(bpy)_2ppb^{\bullet-}]^{+}$, or the reduced ligand, $ppb^{\bullet-}$, show no significant difference in their mean absolute deviation.

The main calculated structural changes on going from parent to reduced species for $[Ru(bpy)_2ppb]^{2+}$ and $[Ru(CN)_4ppb]^{2-}$ lie at r_8 and r_{10} on both chelating and nonchelating sides of the ligand (Table 4). The calculated changes in bond length on going from ppb to $ppb^{\cdot-}$ are larger in $[Ru(bpy)_2ppb]^{2+}$ than $[Ru(CN)_4ppb]^{2-}$. This is a result of the greater skewing of the SOMO of the $ppb^{\bullet-}$ in $[Ru(bpy)_2ppb]^{2+}$ toward the chelated side (Figure 3). The structural asymmetry of the $ppb^{\bullet-}$ in $[Ru(bpy)_2ppb]^{2+}$ may also be responsible for the large number of vibrational modes that consists of motion of both $ppb^{\cdot-}$ and bpy ligands in the reduced complex.

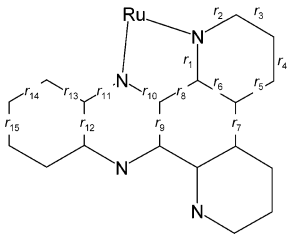

Figure 2. Bond labels for ppb.

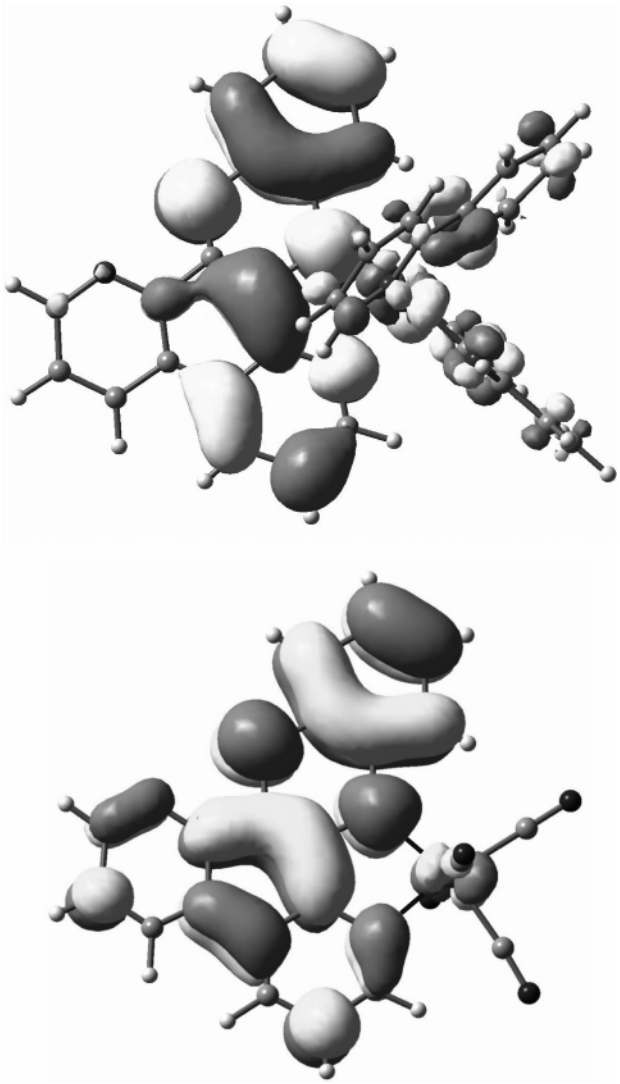

Figure 3. Singly occupied molecular orbitals of (a) $[Ru(bpy)_2(ppb^{\bullet-})]^{+}$ and (b) $[Ru(CN)_4ppb]^{2-*}$.

V. Conclusions

In this paper we report the excited-state lifetimes and transient Raman spectra of $[Ru(bpy)_2ppbX_2]^{2+}$ and transient Raman spectra of $[Ru(CN)_4ppbX_2]^{2-}$, where X = H, Me, Cl. The excited-state lifetimes of the $[Ru(bpy)_2L]^{2+}$ complexes follow the energy gap law; a reduction in lifetime is observed with longer wavelength MLCT absorption transitions. The transient Raman spectra of the $[Ru(CN)_4L]^{2-}$ complexes show a number of differences from their corresponding ground-state spectra. The transient bands, associated with the ppb-based radical anion ligand, shift only modestly from the ground-state vibrations.

This is consistent with density functional theory calculations on the ligand and radical anion. These show that the structural changes on reduction are modest, as are the shifts in the predicted spectra, and that these effects are even less on going from the ground to triplet states of the complexes. The use of the complexes in calculations that model the ground, reduced, and excited states are effective in showing the extent of charge transfer present through NPA calculations. Furthermore, the calculated vibrational spectra of the complexes show a closer correspondence to the experimental data than does the ppb ligand calculation. However, the calculations on the reduced and triplet state of the complexes do not show a significant improvement from $ppb^{\bullet-}$ calculations in terms of predicting the vibrational spectra. The radical anion of the ligand remains an effective model for establishing the spectral properties of the MLCT excited states of the $[Ru(bpy)_2L]^{2+}$ and $[Ru(CN)_4L]^{2-}$ complexes.

Acknowledgment. Support from the Foundation for Research, Science & Technology, the MacDiarmid Institute for Advanced Materials and Nanotechnology, and the University of Otago is gratefully acknowledged. We also acknowledge Drs. A. Flood and M. Polson and Ms. G. David for supplying some of the compounds used in this study.

Supporting Information Available: Tables S1−S5. This material is available free of charge via the Internet at http://pubs.acs.org.

References and Notes

(1) Gardner, J. S.; Strommen, D. P.; Szulbinski, W. S.; Su, H.; Kincaid, J. R. *J. Phys. Chem. A* **2003**, *107*, 351.

(2) Akasaka, T.; Inoue, H.; Kuwabara, M.; Mutai, T.; Otsuki, J.; Araki, K. *Dalton Trans.* **2003**, 815.

(3) Kalyanasundaram, K.; Gratzel, M. *Coord. Chem. Rev.* **1998**, *177*, 347.

(4) Bignozzi, C. A.; Argazzi, R.; Kleverlaan, C. J. *Chem. Soc. Rev.* **2000**, *29*, 87.

(5) Islam, A.; Sugihara, H.; Hara, K.; Pratap Singh, L.; Katoh, R.; Yanagida, M.; Takahashi, Y.; Murata, S.; Arakawa, H. *New J. Chem.* **2000**, *24*, 343.

(6) Yanagida, M.; Islam, A.; Tachibana, Y.; Fujihashi, G.; Katoh, R.; Sugihara, H.; Arakawa, H. *New J. Chem.* **2002**, *26*, 963.

(7) Hara, K.; Sugihara, H.; Tachibana, Y.; Islam, A.; Yanagida, M.; Sayama, K.; Arakawa, H.; Fujihashi, G.; Horiguchi, T.; Kinoshita, T. *Langmuir* **2001**, *17*, 5992.

(8) Anderson, P. A.; Keene, F. R.; Meyer, T. J.; Moss, J. A.; Strouse, G. F.; Treadway, J. A. *J. Chem. Soc., Dalton Trans.* **2002**, 3820.

(9) Adamson, A. W. *J. Chem. Educ.* **1983**, *60*, 797.

(10) Dyer, J.; Blau, W. J.; Coates, C. G.; Creely, C. M.; Gavey, J. D.; George, M. W.; Grills, D. C.; Hudson, S.; Kelly, J. M.; Matousek, P.; McGarvey, J. J.; McMaster, J.; Parker, A. W.; Towrie, M.; Weinstein, J. A. *Photochem. Photobiol. Sci.* **2003**, *2*, 542.

(11) Schoonover, J. R.; Bignozzi, C. A.; Meyer, T. J. *Coord. Chem. Rev.* **1997**, *165*, 239.

(12) Bradley, P. G.; Kress, N.; Hornberger, B. A.; Dallinger, R. F.; Woodruff, W. H. *J. Am. Chem. Soc.* **1981**, *103*, 7441.

(13) Caspar, J. V.; Westmoreland, T. D.; Allen, G. H.; Bradley, P. G.; Meyer, T. J.; Woodruff, W. H. *J. Am. Chem. Soc.* **1984**, *106*, 3492.

(14) Schoonover, J. R.; Chen, P.; Bates, W. D.; Dyer, R. B.; Meyer, T. J. *Inorg. Chem.* **1994**, *33*, 793.

(15) Coates, C. G.; Callaghan, P. L.; McGarvey, J. J.; Kelly, J. M.; Kruger, P. E.; Higgins, M. E. *J. Raman Spectrosc.* **2000**, *31*, 283.

(16) Carroll, P. J.; Brus, L. E. *J. Am. Chem. Soc.* **1987**, *109*, 7613.

(17) Liard, D. J.; Busby, M.; Farrell, I. R.; Matousek, P.; Towrie, M.; Vlcek, A., Jr. *J. Phys. Chem. A* **2004**, *108*, 556.

(18) Gordon, K. C.; McGarvey, J. J. *Inorg. Chem.* **1991**, *30*, 2986.

(19) Omberg, K. M.; Schoonover, J. R.; Meyer, T. J. *J. Phys. Chem. A* **1997**, *101*, 9531.

(20) Schoonover, J. R.; Omberg, K. M.; Moss, J. A.; Bernhard, S.; Malueg, V. J.; Woodruff, W. H.; Meyer, T. J. *Inorg. Chem.* **1998**, *37*, 2585.

(21) Perng, J. H.; Zink, J. I. *Inorg. Chem.* **1990**, *29*, 1158.

(22) Damrauer, N. H.; Weldon, B. T.; McCusker, J. K. *J. Phys. Chem. A* **1998**, *102*, 3382.

(23) Howell, S. L.; Gordon, K. C. *J. Phys. Chem. A* **2004**, *108*, 2536.

(24) Dattelbaum, D. M.; Martin, R. L.; Schoonover, J. R.; Meyer, T. J. *J. Phys. Chem. A* **2004**, *108*, 3518.

(25) Treadway, J. A.; Loeb, B.; Lopez, R.; Anderson, P. A.; Keene, F. R.; Meyer, T. J. *Inorg. Chem.* **1996**, *35*, 2242.

(26) Thompson, D. W.; Schoonover, J. R.; Meyer, T. J.; Argazzi, R.; Bignozzi, C. A. *J. Chem. Soc., Dalton Trans.* **1999**, 3729.

(27) Claude, J. P.; Omberg, K. M.; Williams, D. S.; Meyer, T. J. *J. Phys. Chem. A* **2002**, *106*, 7795.

(28) Howell, S. L.; Matthewson, B. J.; Polson, M. I. J.; Burrell, A. K.; Gordon, K. C. *Inorg. Chem.* **2004**, *43*, 2876.

(29) Polson, M. I. J.; Howell, S. L.; Flood, A.; Blackman, A. G.; Gordon, K. C. *Polyhedron* **2004**, *23*, 1427.

(30) Browne, W. R.; O'Connor, C. M.; Hughes, H. P.; Hage, R.; Walter, O.; Doering, M.; Gallagher, J. F.; Vos, J. G. *J. Chem. Soc., Dalton Trans.* **2002**, 4048.

(31) Bignozzi, C. A.; Chiorboli, C.; Indelli, M. T.; Rampi Scandola, M. A.; Varani, G.; Scandola, F. *J. Am. Chem. Soc.* **1986**, *108*, 7872.

(32) Brewer, K. J.; Murphy, W. R., Jr.; Petersen, J. D. *Inorg. Chem.* **1987**, *26*, 3376.

(33) Hunt, J. W.; Thomas, J. K. *Radiat. Res.* **1967**, *32*, 149.

(34) M. J. Frisch, G. W. T., H. B. Schlegel, G. E. Scuseria, M. A. Robb, J. R. Cheeseman, J. A. Montgomery, Jr., T. Vreven, K. N. Kudin, J. C. Burant, J. M. Millam, S. S. Iyengar, J. Tomasi, V. Barone, B. Mennucci, M. Cossi, G. Scalmani, N. Rega, G. A. Petersson, H. N., M. Hada, M. Ehara, K. Toyota, R. Fukuda, J. Hasegawa, M. Ishida, T. Nakajima, Y. Honda, O. Kitao, H. Nakai, M. Klene, X. Li, J. E. Knox, H. P. Hratchian, J. B. Cross, C. Adamo, J. Jaramillo, R. Gomperts, R. E. Stratmann, O. Yazyev, A. J. Austin, R. Cammi, C. Pomelli, J. W. Ochterski, P. Y. Ayala, K. Morokuma, G. A. Voth, P. Salvador, J. J. Dannenberg, V. G. Zakrzewski, S. Dapprich, A. D. Daniels, M. C. Strain, O. Farkas, D. K. Malick, A. D. Rabuck, K. Raghavachari, J. B. Foresman, J. V. Ortiz, Q. Cui, A. G. Baboul, S. Clifford, J. Cioslowski, B. B. Stefanov, G. Liu, A. Liashenko, P. Piskorz, I. Komaromi, R. L. Martin, D. J. Fox, T. Keith, M. A. Al-Laham, C. Y. Peng, A. Nanayakkara, M. Challacombe, P. M. W. Gill, B. Johnson, W. C., M. W. Wong, C. Gonzalez, and J. A. Pople. Gaussian 03; Gaussian, Inc.: Pittsburgh, PA, 2003.

(35) McClanahan, S. F.; Dallinger, R. F.; Holler, F. J.; Kincaid, J. R. *J. Am. Chem. Soc.* **1985**, *107*, 4853.

(36) Whittle, C. E.; Weinstein, J. A.; George, M. W.; Schanze, K. S. *Inorg. Chem.* **2001**, *40*, 4053.

(37) Yoblinski, B. J.; Stathis, M.; Guarr, T. F. *Inorg. Chem.* **1992**, *31*, 5.

(38) The transient absorption spectra of each of the $[Ru(CN)_4(L)]^{2-}$ are similar showing positive transient absorption from 350 to 480 nm with a negative transient absorption at about 530 nm and a weak positive absorption beyond 650 nm. Single-color experiments at 532 nm showed bleaching of the ground-state features but no obvious excited-state bands—consistent with the reduced absorption, hence resonance effect, at 532 nm in the excited state.

(39) With a 1 mm penetration of the sample and a 300 micron spot size then a 10 mM solution contains 4×10^{14} molecules. A typical pulse energy of 3.6 mJ of 355 nm light contains 6×10^{15} photons. The photon:molecule ratio suggests a complete conversion of the irradiated volume to the excited state.

(40) Gordon, K. C.; McGarvey, J. J. *Chem. Phys. Lett.* **1989**, *162*, 117.

(41) Scott, S. M.; Gordon, K. C.; Burrell, A. K. *Inorg. Chem.* **1996**, *35*, 2452.

(42) Waterland, M. R.; Simpson, T. J.; Gordon, K. C.; Burrell, A. K. *J. Chem. Soc., Dalton Trans.* **1998**, 185.

(43) Matthewson, B. J.; Flood, A.; Polson, M. I. J.; Armstrong, C.; Phillips, D. L.; Gordon, K. C. *Bull. Chem. Soc. Jpn.* **2002**, *75*, 933.

(44) Jameson, R. F. Coordination chemistry of copper with regard to biological systems. In *Metal Ions in Biological Systems*; Sigel, H., Ed.; Marcel Dekker Inc.: New York, 1981; Vol. 12, Chapter 1.